Sensors and Actuators Reports 4 (2022) 100082

Contents lists available at ScienceDirect

Sensors and Actuators Reports

journal homepage: www.sciencedirect.com/journal/sensors-and-actuators-reports

Enhanced Electrochemiluminescence from 3D Nanocavity Electrode Arrays

Loanda Cumba [a,*], Yann Pellegrin [b], Federica Melinato [b], Robert J. Forster [a,*]

[a] National Centre for Sensor Research, School of Chemical Sciences, Dublin City University, Dublin 9, Ireland. FutureNeuro SFI Research Centre
[b] Université de Nantes, CEISAM, UMR CNRS 6230 UFR sciences and techniques, Nantes, France

ARTICLE INFO

Keywords:
Electrochemiluminescence
nanocavity
nanostructured electrode
bipolar electrochemistry
DNA assay
plasmonic enhancement

ABSTRACT

3D arrays comprising interconnected voids have been created using nanosphere lithography (2000≤diameter≤240 nm) followed by electrodeposition of gold. The top surface was blocked with 11-mercaptoundecanoic acid and then the templating polystyrenes were dissolved using THF. The interior surfaces were then functionalized with DNA capture strands that are complementary for part of a target sequence associated with methicillin-resistant *Staphylococcus aureus*, MRSA, genomic DNA. Once the target is hybridised, a probe sequence that is functionalised with $[Ru(bpy)_2\ PIC]^{2+}$, is hybridised to the overhang of the target, bpy is 2,2'-bipyridyl and PIC is (2,2′-bipyridyl)-2(4-carboxy phenyl) imidazo [4,5][1,10] phenanthroline. The electrochemiluminescence, ECL, intensity generated from the hybridised ruthenium dye in the presence of tri-propyl amine and normalised for the charge passed depends on the size of the nanocavity. Significantly, the normalised ECL intensity is approximately 7-fold higher for the 820 nm array than either the 2000 nm array or a planar electrode. The array that is functionalised with the capture-target-Ru probe can be used as a 3D bipolar electrode to wirelessly generate ECL. The peak shape and intensity of the wireless ECL spectra depend on the cavity size with the brightest ECL being observed for the 820 nm cavity array. The results are consistent with a fraction of the ECL light activating the broad cavity plasmon of the array and enhancing the overall ECL intensity. The 820 nm array has been used to develop an assay for the detection of MRSA DNA giving a linear dynamic range from 10 nM to 30 μM with an LOD of 1 μM and an LOQ of 3.2 μM. Significantly, the analytical sensitivity of the wireless ECL assay is approximately 7 times higher for the 820 nm array than that observed for a planar electrode.

1. Introduction

Electrochemiluminescence [1], ECL, where light from a luminophore is generated using electrochemically driven redox processes, offers highly selective detection when the luminophore is conjugated to biorecognition molecules including proteins, antibodies and nucleic acids [2,3,4]. The approach has an extremely high signal to noise ratio [5] because the background is dark and no optical excitation is needed, as well as a broad dynamic range and excellent temporal resolution [6,7]. Nanomaterials [8] and nanostructured surfaces [9] can significantly enhance the intensity of optical responses, e.g., Raman and emission, if the molecules are located within the near field. While particles can deliver significant enhancements, up to 10^{14} in the case of surface enhanced Raman spectroscopy [10], 3D metal nanostructures offer a more reliable platform for the development of analytical sensors and devices [11]. A wide range of ordered nanostructured metal surfaces support localized surface plasmons including nanocavity arrays, metal gratings, and colloidal particle arrays. The primary focus of metal enhanced fluorescence has been on the impact of the plasmonic electric field on *excitation* where the emission intensity is enhanced due to resonance of the exciting radiation with the plasmon of the metal structure. The situation with ECL is different since no optical excitation occurs. However, by tuning the plasmon into resonance with the ECL generated light it ought to be possible to use *a fraction of the light generated by ECL to excite the plasmon of the metal nanostructure* [12]. As we have demonstrated in metallopolymers [13,14,15,16], the key to enhanced ECL intensity (to enable more sensitive detection) is to improve the overall current-to-light conversion efficiency. Under these conditions, the ECL efficiency, ϕ_{ECL}, can be defined as:

$$\phi_{ECL}(x) = \gamma_{ex}(x) * Q * CE(x) \quad (1)$$

where γ_{ex} is the excitation rate of the ECL luminophore that depends on its position, x, (relative to the nanostructure), Q is the ECL quantum

* Corresponding author,
E-mail address: Robert.Forster@DCU.IE (R.J. Forster).

https://doi.org/10.1016/j.snr.2022.100082
Received 3 December 2021; Received in revised form 27 January 2022; Accepted 28 January 2022
Available online 4 February 2022

yield and CE(x) is the collection efficiency Eq. (1)-(2).

For small amplitudes of the electric field, E, where the excitation rate is far from saturation, $\gamma_{ex}(x)$ depends on the strength of the electric field:

$$\gamma_{ex}(x) \propto |E \cdot \mu_{ab}|^2 \quad (2)$$

After excitation, the ECL luminophore can return to its ground state by emitting a photon at a longer wavelength λ_{em} with a radiative decay rate, γ_r or vibrationally relax with a non-radiative decay rate, γ_{nr}. In the presence of a gold nanostructures, *both* γ_r and γ_{nr} ($= \gamma_{nr}^0 + \gamma_{abs}$, where γ_{abs} is the absorption rate) are changed due to the increased local density of optical states at λ_{em} that is associated with plasmon-enhanced field intensity |E| [2]. These changes lead to a modified quantum yield for electrochemiluminescence [17]. When the separation between the nanoparticle and the ECL luminophore is small (< 10 nm), strong quenching is expected due to Förster energy transfer between a fluorophore and a metal. This quenching is accompanied with a metal-enhanced non-radiative decay rate that competes with the desired radiative pathway and shortens the lifetime of the excited state of the ECL luminophore and decreases the quantum yield of emission. For distances that are beyond the quenching zone, but within the decay length of surface plasmon field, emission via surface plasmons dominates and the radiative decay rate can be enhanced [17].

Within this context, nanocavity arrays are highly attractive since they support both surface plasmons and void/nanocavity localized plasmons that can be tuned by varying the cavity size, e.g., through nanosphere lithography [18,19,20]. By functionalising the surface with antibody or nucleic acid capture agents, sandwich assays can then be performed within the cavity giving a potentially enhanced ECL response. Moreover, by using macroscopic samples of the nanostructured materials it ought to be possible to drive enhanced ECL wirelessly using an electric field generated using external feeder electrodes in a closed bipolar electrochemical cell [21]. This approach opens interesting new possibilities. For example, conventional bipolar electrochemistry [22] uses a pair of planar feeder electrodes to create an essentially uniform electric field within a solution that has either low, or no, deliberately added electrolyte and induces a uniform potential gradient within the bipolar electrode. This potential can then drive electrochemiluminescence in elegant new ways [23,24]. However, 3D structured electrodes [25,26], such as nanocavity arrays [27], should focus and shape the electric field opening up a significant new strategy to enhance the performance of bipolar electrochemical and electrochemiluminescence detection.

In this contribution, we describe the use of 3D nanocavity array electrodes in which the pore diameter ranges from 240 to 2000 nm, as bipolar electrodes for the wireless ECL detection of methicillin-resistant *Staphylococcus aureus*, MRSA, genomic DNA. Rapid, point-of-use nucleic acid assays of this type play a key role in early detection of bacterial and viral infections [28] as well as DNA damage [29]. The interior of the cavities is selectively modified with a capture strand that is complementary to part of the target and then a probe strand, labelled with a ruthenium poly-pyridyl type dye, hybridises to the overhang of the target. Here, we show that even at sub-micromolar concentrations of the target, ECL is observed when the probe strand hybridises. Significantly, the ratio of ECL intensity to charge passed depends on the size of the cavities and can exceed the intensity observed for planar electrode surfaces by as much as 8-fold. These results suggest that the Ru electrochemiluminescence at approximately 610 nm can excite the cavity plasmon thus enhancing the ECL intensity of a fraction of the immobilised luminophores.

2. Materials and methods

2.1. Gold nanocavity arrays

Gold nanocavity arrays with diameters of 240, 430, 600, 820, 1000 and 2000 nm were prepared on gold coated silicon wafers (Amsbio) using nanosphere lithography as described previously [18,19]. Briefly, the gold electrodes were cleaned by placing them in piranha solution (3:1 mixture of sulphuric acid and 30% hydrogen peroxide, *(caution, this mixture reacts violently with organic material!)* for 20 min, followed by thorough rinsing with ultra-pure water. The electrode was then scanned between -0.300 V and +1.300 in 0.01 M H_2SO_4 to form and subsequently reduce an oxide monolayer to measure the surface roughness of the gold electrode and to remove any adventitious adsorbates. Between 3 and 5 hexagonally close packed layers of polystyrene spheres (Bangs Laboratories) were assembled on the clean gold-coated silicon wafer. Gold (Technic Inc. Sodium gold sulphite solution, Cranston, RI, USA) was then electrodeposited at -0.95 V versus an Ag/AgCl reference (sat. KCl) electrode through the sphere array to a thickness that is 75-80% of the diameter of the top layer of spheres. Following gold deposition, a monolayer of 11-mercaptoundecanoic acid, MUA, was formed on the top surface with the templating spheres in place, by immersing the nanocavity array in 1 mM of MUA in ethanol for 12 h. This is to block any binding of the capture DNA capture strands to the top surface of the nanocavity array thus avoiding any contribution from the top surface plasmons. The polystyrene spheres are then removed by sonication in THF for 30 minutes. Complete sphere removal is confirmed by the absence of polystyrene bands in the Raman spectrum of the array. Raman spectra were recorded using 633 nm laser line (laser intensity was 0.4 mW) using a 50x objective and an acquisition times of 5 s. A minimum of five replicate samples were measured to ensure that representative spectra are obtained.

The structure of the arrays was characterised using a Bruker Dektak XT Stylus Profilometer and a Bruker Dimension 3100 AFM equipped with a NanoScope IIIa controller using a silicon nitride tip with a tip diameter of 20 nm operating in contact mode. The topology of the nanocavity array structures were also investigated using a Hitachi S5500 Field Emission Scanning Electron Microscope. SEM image analysis was carried out using Image J software.

2.2. Electrochemistry and electrochemiluminescence

All conventional electrochemical experiments were performed using a CH Instruments, Model 760B Electrochemical Workstation in a three-electrode cell at 23 C comprising the gold nanocavity array, or a 3 mm diameter gold disk electrode (CH Instruments), as the working electrode, a CH Instruments silver/silver chloride (Ag/AgCl) as the reference electrode and a platinum wire (Sigma Aldrich) as the counter electrode.

For bipolar experiments, two titanium plates (1 cm x 1 cm) were used as feeder electrodes and a direct current power supply (Tenma Bench, Output 0 to 30 V dc, 0 to 2A) was employed to generate the electric field required.

The intensity of the ECL was measured with an Oriel 70680 photomultiplier tube (PMT) biased at -850 V using a high-voltage power supply (Oriel, Model 70705) and an amplifier/recorder (Oriel, Model 70701). In wireless electrochemiluminescence, spectra were collected using a Keyence 3D digital Microscope connected to an 77400 MS125 spectrograph and an Andor Technology gated intensified CCD. Confocal imaging was carried out using a Leica TSP DMi8 confocal microscope with immersion objective lenses between 10 and 100 x.

2.3. Nucleic acid assay

The oligonucleotides were purchased from Eurogentec (98 %), Belgium. The probe used in this work was a 5' thiol modified oligonucleotide probe (5'-GTAGAAATGACT-GAACGTCCGATAA-3') (Probe 1) which targets the mecA gene segment found in MRSA [30].

2.4. Labelling of probe strand

The reaction was carried out in two steps. First, Ru PIC-COOH was

dissolved in DMSO with a molar equivalent of sodium-4-((4-(cyanoethynyl)benzoyl)oxy)-2,3,5,6-tetrafluorobenzenesulfonate (CBTF) and stirred for approximately 10 minutes at room temperature. A molar equivalent aliquot was then added to the amino terminated DNA probe strand (Probe 2) in PBS (pH 7.4) and stirred for a minimum of 60 minutes. The Ru-probe DNA was purified using the QIAquick® PCR Purification Kit (Qiagen, Valencia, CA, USA) per the manufacturer's protocol. The DNA was eluted in water or 1 mM Tris-HCl buffer, pH 8.5. The DNA was precipitated with the addition of 0.1 volume of 3 M sodium acetate, pH 5.2, and 2 volumes of absolute ethanol.

2.5. DNA assay

Denhardt's Hybridisation solution (≥99.5%) was used for DNA immobilisation and hybridisation and was used as received from Sigma Aldrich. The nanocavity arrays were functionalised with the capture strands by immersing in a 1 μM solution of the thiolated DNA in Denhardt's solution for 14 hours at 37 C. The arrays were then repeatedly (5 x) emersed, washed with buffer and then soaked in buffer for 20 minutes to remove any unbound material. Hybridization of the target DNA strand to the capture strand was performed at 37°C for 3 h. The probes strands, functionalised with the ruthenium dye were hybridized with the complementary section of the target not used for binding to the capture strand for 5 h at 37°C.

3. Results and discussion

3.1. Nanocavity array structure

Fig. 1A shows an SEM of the 830 nm gold nanocavity arrays revealing well-ordered, hexagonal close packed, 3D, arrays are formed that has a low defect density (<1 defect per 500 cavities) over an area of approximately 25 mm^2 in the case of larger spheres or 10 mm^2 for the smaller spheres (<600 nm). The three-fold voids that interconnect the discrete layers are clearly visible suggesting that the arrays have significant porosity.

3.2. Optical properties

As discussed previously [18,31], the nanocavity arrays are less reflective than smooth gold and the arrays absorb significantly at wavelengths longer than approximately 550 nm. While the arrays themselves are structurally well ordered, a well-defined peak associated with a localised plasmon is not observed because multiple cavity and surface plasmons overlap to give a broad absorbance. Given that the ruthenium complex emits at approximately 620 nm, it is possible that a fraction of the ECL generated light could be used to excite the plasmons of the nanovoid arrays. However, several parameters and processes, including the electrode area, luminophore surface coverage, as well as the electron and mass transport rates, influence the brightness of electrochemiluminescence. Conventional electrochemistry can provide deep insights into these issues.

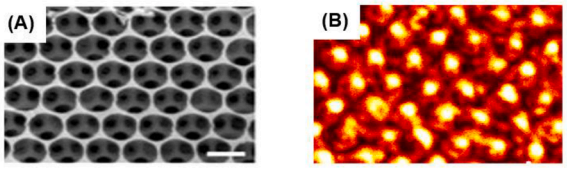

Fig. 1. (A) SEM image of the 600 nm gold nanocavity array using a 10 kV accelerating voltage. The scale bar is 800 nm. (B) Wireless electrochemiluminescence following the formation of the DNA capture-target-Ru labelled probe where the target concentration is 1 μM and the TPA concentration is 25 mM within a porous electrode containing interconnected spherical voids with a diameter of 820 nm. This image is collected at the anode end of the bipolar electrode and the electric field gradient is small at these length scales hence there is little variation in the emission intensity from right to left.

3.3. Electrochemical properties

Successful immobilisation of the capture strand followed by hybridisation of the target and ruthenium dye labelled probe strands can be conveniently monitored using cyclic voltammetry since the metal complex undergoes a one-electron oxidation at approximately +1.05 V [32]. The microscopic or real area, A_{Real}, of each nanocavity array has been measured by forming an oxide monolayer using voltammetry in 0.1 M H_2SO_4. This area allows the current density to be determined which should be independent of the size of the nanocavities. As illustrated in Fig. 2, incubation of the capture strand modified array with 1 μM target and then the Ru-probe gives a well-defined voltammetric peak at +1.05 V which is consistent with the $Ru^{2+/3+}$ redox process. The peak shape is approximately gaussian, shows a ratio of anodic, i_{pa}, to cathodic, i_{pc}, currents of between 0.9 and 1.05, a full width at half maximum, FWHM, of 110 mV and the current increases linearly with increasing scan rate, υ, for $0.002 \leq \upsilon \leq 0.1000$ V s^{-1}. The peak-to-peak separation, ΔE_P, is 55±10 mV but is independent of υ, for $0.002 \leq \upsilon \leq 0.1000$ V s^{-1} suggesting that slow heterogeneous electron transfer is not the origin of the non-zero ΔE_P. These features are consistent with immobilisation of the Ru-probe through the formation of the capture-target-Ru probe within the cavities [33].

However, it is very important to note that finite diffusion [34] of *solution phase* Ru-probe within the cavities would be expected at scan rates *slower* than approximately 12 Vs^{-1} (2000 nm cavities) or 1200 Vs^{-1} (240 nm cavities) because of the very small volumes of the cavities, i.e., 10^{-15} to 10^{-18} litres. Thus, very careful washing of the nanocavity array is essential to ensure that the Ru-probe is truly bound and that the response is not due to residual Ru-probe. The inset of Fig. 2 shows the dependence of the charge under the voltammogram, Q, divided by A_{Real} (as measured using oxide monolayer formation/reduction in acidic electrolyte) on the number of wash cycles. Here, the arrays functionalised with the capture strand have been immersed in a 1 μM solution of the target followed by 500 μM of the Ru-probe. This figure shows that ratio initially depends on the cavity size, but the three cavity sizes converge to a single value (±12%) after four wash cycles. This behaviour is consistent with the cavity initially being filled with 500 μM of the Ru-probe which gets washed out leaving a partial monolayer of Ru-probe that is hybridised to the target. The data show that the zero wash cycle Q/A_{Real} value is statistically larger for the larger (2 μm) cavity array which is consistent with the larger total number of moles of

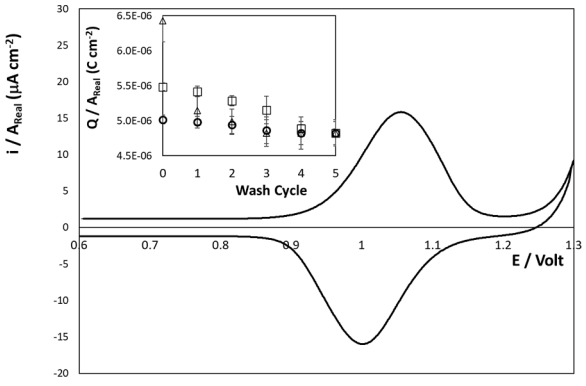

Fig. 2. Cyclic voltammogram of the 820 nm cavity array following the formation of the DNA capture-target-Ru labelled probe where the target concentration is 1 μM and the capture probe is 50 μM. The array was washed (5x) before the voltammogram was recorded. The scan rate is 0.1 V s^{-1} and the current density is determined using the real array area. The inset shows the dependence of the charge passed in the CV as a function of the wash cycle. The cavity sizes are: Δ, 2000 nm; □, 820 nm and ◯ 240 nm.

Ru-probe in solution within the cavity. However, the dependence of the normalised charge on the wash cycle cannot be quantitatively analysed because the efficiency of the wash step depends on the size of the cavity opening. Significantly, when the pristine cavity, i.e., where the deposition of the capture strand step is omitted, is exposed to first the target and then the Ru labelled probe strand, no redox processes associated with $Ru^{2+/3+}$ are observed. This negative control indicates that non-specific adsorption of the Ru-probe is not a significant issue and that the Ru-probe can be introduced into the cavities and washed out again. Overall, these data suggest that the capture strand has been successfully immobilised on the surface of the cavity interiors and that the target and Ru-probe strands can hybridise. Based on the limiting value of Q/A_{Real}, the surface coverage of Ru is approximately 5×10^{-11} mol cm^{-2} where the target concentration is 1 μM, which, if the capture strands are close packed would correspond to approximately 50% of the capture strands being hybridised to targets.

3.4. Conventional electrochemiluminescence

Fig. 3 shows the ECL response for the nanocavity arrays where the cavity size is varied from 2000 to 240 nm. The onset of ECL occurs at approximately 0.8 V. Given the formal potential of the $Ru^{2+/3+}$ couple is approximately +1.05 V the concentration of electrogenerated Ru^{3+} will be low at this onset potential and the ECL at these low potentials is most likely generated by the reaction of the TPA radical cation with Ru^{2+}. This chemical oxidation pathway will be promoted by the use of a high TPA concentration, i.e., 50 mM. The ECL response shows a well-defined peak with a pronounced diffusional tail rather than a steady state response. This behaviour is consistent with depletion of the TPA co-reactant within the nanocavities which is reasonable given that, in the absence of slow heterogeneous electron transfer, the depletion layer thickness at 0.1 V s^{-1} is approximately 11 μm, i.e., more than 5 times larger than the diameter of the largest nanocavities investigated. It is important note that the total amount of ruthenium dye bound within the cavities depends on their size. To create the ECL luminophore, the bound Ru^{2+} dye must be oxidised, and the charge passed in the CV recorded at the same time as the ECL response reflects the differences in the total moles of the ruthenium dye present. Therefore, we have normalised the ECL intensity by dividing the ECL intensity, I_{ECL}, by the charge passed, Q, to estimate the photons emitted per electron passed due to oxidation of Ru^{2+}. A striking result of Fig. 3 is that even after correcting for the charge passed, the ECL intensity depends on the size of the nanocavity and can be significantly larger than that observed at a planar electrode. It is important to recognise that ECL is a complex process involving heterogeneous electron transfer, mass transport and cross-reaction of reactants in solution. However, voltammetry suggests that the standard heterogeneous electron transfer from Ru^{2+} does not influence the ECL intensity at 0.1 Vs^{-1}. Moreover, as shown in the inset of Fig. 3, the normalised ECL intensity does not vary systematically with the cavity size which would be expected if transport effects dominated, e.g., trapping of the electrogenerated radicals within the cavity to give a higher local concentration. Significantly, the enhancement factor, i.e., the ratio of the normalised ECL intensity for the nanocavity array relative to a planar electrode, reaches a maximum value of 6.6±1.3 for the 820 nm cavity array. These data are consistent with plasmonic enhancement of the electrochemiluminescence in which some of the 610nm ECL excites the cavity plasmon and the augmented local electric field enhances the emission.

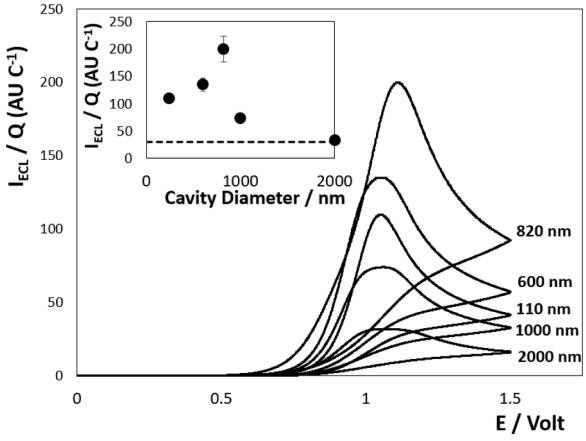

Fig. 3. Potential dependence of the of the ECL intensity normalised for the charge passed for nanocavity arrays where the cavity sizes, from top to bottom at +1.5 V are, 820, 600, 110, 1000 and 2000 nm. The arrays have been functionalised with the capture strand, a 1 μM solution of the target allowed to hybridise, and the target overhang labelled using a 50 μM solution of the Ru-probe strand. Prior to measurement, the arrays were washed 5 times to remove unbound Ru-probe (see inset of Fig. 2). The scan rate is 0.1 Vs^{-1} and the TPA concentration is 50 mM. The inset shows the dependence of the peak ECL intensity normalised for the charge passed on the cavity size. The dashed line represents the ECL intensity observed for a planar electrode.

Generating electrochemiluminescence wirelessly by applying an electric field using external feeder electrodes is a highly attractive strategy for diverse applications including remote monitoring and highly sensitive, multianalyte, detection [35]. 3D bipolar electrodes open new possibilities including the possibility of focusing the electric field to create non-uniform potentials, pre-concentrating electrogenerated reagents, avoiding convection and controlling diffusional mass transport. Moreover, it may be possible to couple the electric field created within the bulk solution and the local electric field of the plasmon.

3.5. Wireless electrochemiluminescence

Fig. 4 shows ECL spectra obtained for a 0.5 cm x 0.5 cm sample of the nanocavity arrays where the electric field strength is 6 V cm^{-1}. If the voltage drops linearly between the two feeder electrodes, this field strength will induce a voltage difference of 3 V between the anodic and cathodic poles of the nanocavity array (±1.5 V). The voltage at the

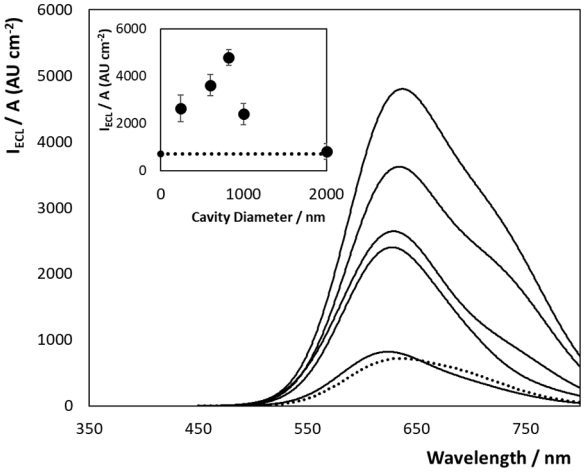

Fig. 4. Spectra for wireless electrochemiluminescence generated from an 0.5 cm x 0.5 cm sample of the nanocavity arrays placed within a 6 V cm^{-1} electric field. The cavity sizes, from top to bottom at 620 nm are, 820, 600, 110, 1000 and 2000 nm. The arrays have been functionalised with the capture strand, a 1 μM solution of the target allowed to hybridise, and the target overhang labelled using a 50 μM solution of the Ru-probe strand. Prior to measurement, the arrays were washed 5 times to remove unbound Ru-probe (see inset of Fig. 2). The TPA concentration is 50 mM. The inset shows the dependence of the peak ECL intensity normalised for the area of the cavity array as measured using oxide monolayer formation/reduction. The dashed line represents the ECL intensity observed for a planar electrode.

anode should be sufficient to oxidise Ru^{2+} while oxygen or water is reduced at the cathode. The ECL spectra are centred at 630±8 nm while that found using optical excitation is 620±5 nm. These minor shifts most likely arise due to the different local microenvironment of the luminophore when hybridised within the nanocavity compared to dissolved in bulk solution or lateral, inter-molecular interactions. The ECL spectra are consistent with phosphorescence from the triplet MLCT state [36]. There are differences in the peak shape between the ECL and optically driven emission and the band shape depends subtlety on the cavity size with the high energy side becoming relatively less intense compared to the emission at longer wavelength. This behaviour is consistent with a fraction of the electrochemiluminescence being absorbed by the nanocavity. Significantly, as observed for conventional ECL, the area normalised intensity of the wirelessly driven depends non-linearly on the cavity size (inset of Fig. 4) with the 820 nm cavities showing an emission intensity approximately 7-times higher than that observed for either the 2000 nm cavity array or a cavity-free planar electrode. While recognising that it is very difficult to quantify the charge associated with the generation of the Ru^{3+} required for emission in a bipolar electrochemical experiment, the data shown in the inset of Fig. 2, i.e., Q/A_{Real} converging to a single value for all arrays following five wash cycles, suggests that the current density is essentially the same for all arrays irrespective of the cavity size. Given that the ECL intensity depends on the current density, this gives confidence that the changes in ECL intensity shown in the inset of Fig. 4 reflect cavity size induced changes in the ECL process other than electron transfer. The results presented in Fig. 4 are significant since they demonstrate that ECL can be generated wirelessly using a 3D electrode array of nanocavities and open the possibility of enhancing the ECL intensity by tuning the cavity size as has been demonstrated previously for optically induced emission [37].

3.6. DNA assay

The surface coverage of the Ru-probe, and hence the wireless ECL intensity, are expected to depend on the concentration of the target DNA. Fig. 5 shows that I_{ECL} / A_{Real} depends linearly on the concentration of the DNA target for the 820 nm microcavity array where the electric field strength is 3 V cm^{-1}. The linear dynamic range extends from 10 nM to 30 μM with an LOD (3.3 * standard deviation of intercept / slope) of 1 μM and an LOQ (10 * standard deviation of intercept / slope) of 3.2 μM.

The absolute slope is approximately 0.91, i.e., the ECL intensity increases by a factor of 1.8 when the concentration is doubled. This value is somewhat lower than the value of unity expected for a direct correlation between the DNA concentration in solution and the number of captured Ru-Probe sequences and hence the ECL brightness. However, Fig. 5 clearly demonstrates that the intensity of the wirelessly generated ECL depends on the target concentration. Moreover, the analytical sensitivity delivered by the nanocavity array is approximately 6 times higher than that achieved by the planar electrode under identical conditions.

4. Conclusions

3-dimensional nanocavity electrode arrays with spherical voids with 240≤diameter≤2000 nm offer significant advantages in both conventional and wireless/bipolar electrochemiluminescence. Significantly, the area and charge corrected electrochemiluminescence intensity is approximately 7-fold higher at the nanostructured electrode than a traditional planar electrode. The enhancement factor depends non-linearly on the cavity size with an optimum diameter of the order of 800 nm. The enhancement does not appear to be related to different rates of heterogeneous charge transfer or mass transport but is consistent with a fraction of the ECL generated light activating the broad cavity plasmons of the array giving rise to an amplified local electric field that enhances the ECL intensity. The cavity induced enhancement translates into an enhanced analytical sensitivity and lower limit of detection in a DNA assay. While significantly lower LODs can be achieved using other electrochemical approaches such as electrocatalytic metal nanoparticles [38], the wireless ECL strategy is attractive from the perspectives of simple, low-cost instrumentation, non-complex, multianalyte capability that can be easily scaled to handle a large panel of biomarkers. The enhancement factor for other dyes, e.g., organics that have a lower quantum yield of emission, could be even larger than those found for the DNA bound ruthenium complexes.

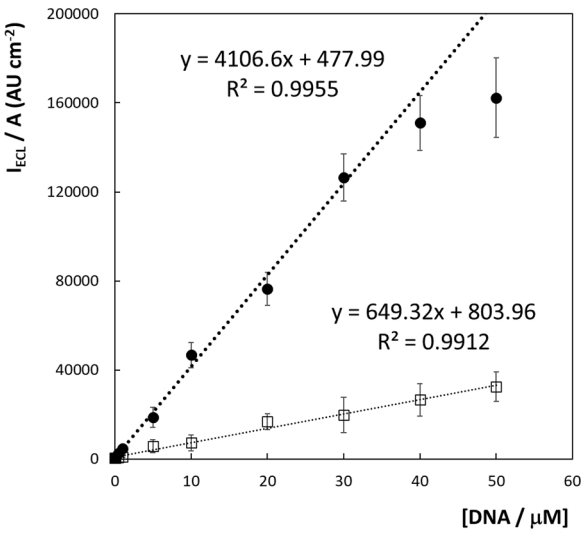

Fig. 5. The dependence of the wirelessly generated ECL intensity at 635 nm on the concentration of the target DNA in solution for an 820 nm cavity array (•) and a planar electrode (□). The conditions are as described in Fig. 4.

Declaration of Competing Interest

The authors whose names are listed immediately below report the following details of affiliation or involvement in an organization or entity with a financial or non-financial interest in the subject matter or materials discussed in this manuscript. Please specify the nature of the confl ict on a separate sheet of paper if the space below is inadequate.

Acknowledgements

This project has received funding from the European Union's Horizon 2020 research and innovation programme under the Marie Skłodowska-Curie Grant Agreement No. 813439. This publication has emanated from research supported in part by a research grant from Science Foundation Ireland (SFI) under Grant Number 16/RC/3948 and co-funded under the European Regional Development Fund and by FutureNeuro industry partners. The financial support of the Environmental Protection Agency (Ireland, Award 2019-W-MS-41) and the Agence Nationale de la Recherche (France, ANR-18-WTW7-0006-05), is gratefully acknowledged.

References

[1] A. Fiorani, G. Valenti, M. Iurlo, M Marcaccio, F. Paolucci Electrogenerated chemiluminescence: A molecular electrochemistry point of view Current Opinion in Electrochem., 8, (2018), pp.31-38, 10.1016/j.coelec.2017.12.005.
[2] JF Rusling, RJ Forster, Biosensors Designed for Clinical Applications, Biomedicines 9 (7) (2021) 702–709, https://doi.org/10.3390/biomedicines9070702.
[3] R.J. Forster, ECL of Nanomaterials: Novel Materials, Detection Strategies and Applications Analytical Electrogenerated Chemiluminescence: From Fundamentals to Bioassays, Sojic, N (2019) 247–273.
[4] S. Rebeccani, C. Wetzl, V.A. Zamolo, A. Criado, G. Valenti, F. Paolucci, M. Prato, Electrochemiluminescent immunoassay enhancement driven by carbon nanotubes, Chem. Commun. 57 (2021) 9672–9675, https://doi.org/10.1039/D1CC03457J.

[5] L Dennany, EJ O'Reilly, TE Keyes, RJ Forster Electrochemiluminescent monolayers on metal oxide electrodes: Detection of amino acids, Electrochem. Commun. 8 (10) (2006) 1588–1594.
[6] M. Bhaiyya, P. Kumar, P. Sanket Goel, A brief review on miniaturized electrochemiluminescence devices: From fabrication to applications Current Opin. in, Electrochem 30 (2021) 100800–110805, https://doi.org/10.1016/j.coelec.2021.100800.
[7] G. Valenti, A. Fiorani, E. Villani, A. Zanut, F. Paolucci, The Essential Role of Electrode Materials in ECL Applications Analytical Electrogenerated Chemiluminescence, 2019, pp. 159-175, 10.1039/9781788015776-00159.
[8] S. Rebeccani, C. Wetzl, V.A. Zamolo, A. Criado, G. Valenti, F. Paolucci, M. Prato, Electrochemiluminescent immunoassay enhancement driven by carbon nanotubes, Chem. Commun. 57 (76) (2021) 9672–9675, https://doi.org/10.1039/D1CC03457J.
[9] E Villani, G Valenti, M Marcaccio, L Mattarozzi, S Barison, D Garoli, S. Cattarin, F. Paolucci, Coreactant electrochemiluminescence at nanoporous gold electrodes, Electrochim. Acta 277 (2018) 168–175, https://doi.org/10.1016/j.electacta.2018.04.215.
[10] P.A. Mercadal, E.R. Encina, J.E.L. Villa, E.A. Coronado, A New Figure of Merit to Assess the SERS Enhancement Factor of Colloidal Gold Nanoparticle Aggregates, J. Phys. Chem. C 125 (7) (2021) 4056–4065, https://doi.org/10.1021/acs.jpcc.0c09122.
[11] S. Kasani, K. Curtin, N. Wu A review of 2D and 3D plasmonic nanostructure array patterns: fabrication, light management and sensing applications Nanophotonics,8 (12) (2019), 2065-2089, 10.1515/nanoph-2019-0158.
[12] J. Ding, P. Zhou, W. Guo, B. Su Confined Electrochemiluminescence Generation at Ultra-High-Density Gold Microwell Electrodes Frontiers in Chem.8 (2021), 630246,10.3389/fchem.2020.630246.
[13] J.J. Walsh, Q. Zeng, R.J. Forster, T.E. Keyes, Highly luminescent Ru(ii) metallopolymers: photonic and redox properties in solution and as thin films, Photochem. Photobiol. Sci. 11 (2012) 1547–1557.
[14] L. Dennany, C.F. Hogan, T.E. Keyes, R.J. Forster, Effect of Surface Immobilization on the Electrochemiluminescence of Ruthenium-Containing Metallopolymers, Anal. Chem. 78 (2006) 1412–1417.
[15] R.J. Forster, J.G. Vos, M.E.G. Lyons, Controlling processes in the rate of charge transport through [Os (bipy) 2 (PVP) n Cl] Cl redox polymer-modified electrodes, J. Chem. Soc., Farad. Trans. 87 (23) (1991) 3761–3767, https://doi.org/10.1039/FT9918703761.
[16] A Devadoss, A.M. Spehar-Déleze, D.A. Tanner, P. Bertoncello, R. Marthi, T.E Keyes, R.J Forster, Enhanced electrochemiluminescence and charge transport through films of metallopolymer-gold nanoparticle composites, Langmuir 26 (3) (2010) 2130–2135, https://doi.org/10.1021/la902676p.
[17] D. Wang, L. Guo, R. Huang, B. Qiu, Z. Lin, G. Chen, Surface Enhanced Electrochemiluminescence of $Ru(bpy)_3^{2+}$, Sci. Rep 5 (2015) 7954, https://doi.org/10.1038/srep07954.
[18] F. Lordan, J.H. Rice, B. Jose, R.J. Forster, T.E. Keyes, Effect of cavity architecture on the surface-enhanced emission from site-selective nanostructured cavity arrays, J. Phys. Chem. C 116 (2) (2012) 1784–1788, https://doi.org/10.1021/jp210343t.
[19] B. Jose, R.K. Vijayaraghavan, L. Kent, S. O'Toole, J. O'Leary, R.J. Forster, Tunable metallic nanostructures using 3D printed nanosphere templates, Electrochem. Commun. 98 (2019) 106–109, https://doi.org/10.1016/j.elecom.2018.12.002.
[20] C.T. Mallon, K.W. Kho, H. Gartite, R.J. Forster, T. E, Keyes Fabrication and Optical Properties of Periodic Ag Nano-Pore and Nano-Particle Arrays with Controlled Shape and Size over Macroscopic Length Scales Adv, Eng. Mats. 20 (1) (2018), 1700532, https://doi.org/10.1002/adem.201700532.
[21] G. Loget, D. Zigah, L. Bouffier, N. Sojic, A. Kuhn, Bipolar electrochemistry: from materials science to motion and beyond Accounts of, Chem. Res. 46 (11) (2013) 2513–2523, https://doi.org/10.1021/ar400039k.
[22] C. Qin, Z. Yue, Y. Chao, R.J. Forster, F. O'Maolmhuaidh, X.F. Huang, S. Beirne, G. G Wallace, J. Chen, Bipolar electroactive conducting polymers for wireless cell stimulation, App. Mat. Today 21 (2020), 100804, https://doi.org/10.1016/j.apmt.2020.100804.
[23] Y. Wang, R. Jin, N. Sojic, D. Jiang, H.-Y. Chen, Intracellular wireless analysis of single cells by bipolar electrochemiluminescence confined in a nanopipette, Angew. Chem., Int. Ed. 59 (2020) 10416–10420, https://doi.org/10.1002/anie.202002323.
[24] J. Dong, Y. Lu, Y. Xu, F. Chen, J. Yang, Y. Chen, J. Feng, Direct imaging of single-molecule electrochemical reactions in solution, Nature 596 (2021) 244–249, https://doi.org/10.1038/s41586-021-03715-9.
[25] S.F. Douman, M.R. De Eguilaz, L.R. Cumba, S. Beirne, G.G. Wallace, Z. Yue, E. I. Iwuoha, R.J. Forster, Electrochemiluminescence at 3D Printed, Titanium Electrodes Frontiers in chem 9 (2021) 279, https://doi.org/10.3389/fchem.2021.662810.
[26] S.F Douman, D. Collins, L.R. Cumba, S. Beirne, G.G. Wallace, Z Yue, Wireless electrochemiluminescence at functionalised gold microparticles using 3D titanium electrode arrays, Chem. Commun. 57 (38) (2021) 4642–4645, https://doi.org/10.1039/D1CC01010G.
[27] C.T. Mallon, R.J. Forster, T.E. Keyes, Fabrication of gold sphere to cuboid nanoarrays using PDMS templates, Chem. Commun. 47 (2011) 7605–7607, https://doi.org/10.1039/c1cc11495f.
[28] M.R. de Eguilaz, L.R. Cumba, R.J. Forster, Electrochemical detection of viruses and antibodies: A mini review Electrochem, Commun 116 (2020), 106762, https://doi.org/10.1016/j.elecom.2020.106762.
[29] I. Bist, S. Bhakta, D. Jiang, T.E. Keyes, A. Martin, R.J. Forster, J.F. Rusling, Evaluating metabolite-related DNA oxidation and adduct damage from aryl amines using a microfluidic ECL array, Anal. Chem. 89 (22) (2017) 12441–12449, https://doi.org/10.1021/acs.analchem.7b03528.
[30] R. Oueslati, Y. Jiang, J. Chen, J. Wu, Rapid and sensitive point of care detection of MRSA genomic DNA by nanoelectrokinetic sensors, Chemosensors 9 (2021) 97, https://doi.org/10.3390/chemosensors9050097.
[31] J. Bincy, R.J. Forster, T.E. Keyes, F. Lordan, J.H. Rice, Site selective surface enhanced Raman on nanostructured cavities, App. Phys. Letts. 99 (2011), 033104, https://doi.org/10.1063/1.3615282.
[32] R.J. Forster, Heterogeneous Kinetics of Metal-and Ligand-Based Redox Reactions within, Adsorbed Monolayers Inorg. Chem. 35 (11) (1996) 3394–3403, https://doi.org/10.1021/ic951343e.
[33] R.J. Forster, T.E. Keyes, Redox properties of ground and electronically excited states:$[Ru(bpy)_2Qbpy]^{2+}$ monolayers J, Phys. Chem. B 102 (49) (1998) 10004–10012, https://doi.org/10.1021/jp9828890.
[34] V. Climent, J.M. Feliu, Cyclic Voltammetry Encyclopedia of Interfacial Chemistry, Surface Science and Electrochemistry (2018) 48–74, https://doi.org/10.1016/B978-0-12-409547-2.10764-4.
[35] L Bouffier, D Zigah, N Sojic, A Kuhn Bipolar (Bio) electroanalysis Ann, Rev. Anal. Chem. 14 (2021) 65–86, https://doi.org/10.1146/annurev-anchem-090820-093307.
[36] K.W. Lee, J.D. Slinker, A.A. Gorodetsky, S. Flores-Torres, H.D. Abruña, P. L. Houston, G. G, Malliaras Photophysical properties of tris(bipyridyl)ruthenium (ii) thin films and devices, Phys. Chem. Chem. Phys. 5 (2003) 2706–2709. /10.1039/B302119J.
[37] U. Neugebauer, E. Sheridan, R. Marthi, B. Jose, R. Steffen, R.J. Forster, T.E. Keyes, Emission enhancement within gold spherical nanocavity arrays, Phys. Chem. Chem. Phys. 11 (2009) 10923–10933, https://doi.org/10.1039/B908385E.
[38] E. Spain, T.E. Keyes, R.J. Forster, DNA sensor based on vapour polymerised PEDOT films functionalised with gold nanoparticles, Biosens. and Bioelectron. 41 (2013) 65–70, https://doi.org/10.1016/j.bios.2012.06.046.